Reconfigurable FSS Based on Movable 3D-Printed Metal-Dielectric Grids

Siyu Li[1], Peter Njogu[1], Benito Sanz-Izquierdo[1], Steven Gao[1], Zhijiao Chen[2]
[1]Division of Computing, Engineering and Mathematical Sciences, University of Kent, Canterbury, UK, sl744@kent.ac.uk
[2]Department of Electronic Engineering, Beijing University of Posts and Telecommunications, Beijing, China

***Abstract*— A reconfigurable frequency selective surface (FSS) based on movable 3D-printed grids is present in this paper. By moving the 3D-printed grid up and down in purposely made channels between two adjacent unit cells, a reconfigurable FSS with different frequency responses could be achieved. The FSS unit with channels and the insertable grids are first simulated and studied using Ansys HFSS. Then a 9 × 9 FSS array with channels is fabricated using standard etching techniques and milling. Finally, the FSS structure and the insertable grids are tested under various conditions. This work aims to demonstrate a new concept for the reconfigurable FSS based on movable metallic and dielectric grids. These are based on low-cost, high-flexibility, and ease-of-fabrication 3D printing technique, and provide a new path for designing reconfigurable FSSs by inserting and removing materials with different electrical properties to achieve different frequency responses.**

***Index Terms*—frequency selective surface (FSS), 3D printing, additive manufacturing, transmission response.**

I. Introduction

A Frequency Selective Surface (FSS) is a periodic electromagnetic (EM) filtering structure that is used to modify an incident EM wave and provide dispersive transmission or/and reflection characteristics [1]. Their frequency responses are dependent on the geometry and spacing of the elements, dielectric material thickness and properties, as well that of its surroundings [2]. In practical, FSS has been extensively utilized in a wide range of applications, such as electromagnetic interference (EMI) shielding, absorbers, antenna reflectors, and hybrid high performance radomes [3-6]. In recent years, the demand for multifunctional EM structures such as FSS that work well at multiple frequency bands has been increasing due to the rapid development of the emerging modern wireless communication systems,.

Frequency reconfigurability is one of the most desired features of an antenna in advanced communication systems [7]. Electronic reconfigurability is usually achieved by incorporating switches, variable capacitors, phase shifters, or ferrite materials in the topology of the antenna [8]. Most frequently , lumped components such as PIN diodes, varactor diodes, or micro-electro-mechanical systems (MEMS) switches or varactors are used in the design of reconfigurable antennas [9]. More recently, the use of precision piezo-electrical actuators have open the opportunity of developing movable surfaces that can achieve reconfiguration [10].

In recent years, emerging 3D printing (or called additive manufacturing) technique has attracted a lot of attention as an advanced fabrication process due to its advantages of low cost, high flexibility, more degrees of freedom (DoF), and ease of fabrication. It has been broadly applied to a wide range of industrial and research areas such as antenna design, RF component fabrication and promoted the development of joint subjects [11, 12]. In this way, combining the 3D printing technique with FSS may be a good solution for designing the RF components in a low-cost, high-integration and high-flexibility way.

This paper presents a FSS that uses movable 3D-printed metal and dielectric grids to achieve frequency reconfigurability. A bandstop square loop FSS with channels between its adjacent units is first simulated and analyzed, then a corresponding 9 × 9 units array FSS is fabricated to create a basic structure. A 3D-printed dielectric and metal-dielectric grid are both fabricated to be combined with the basic FSS to form the frequency reconfigurable FSS. The combined structure was measured using standard transmission measurement platform. The measured results show a good agreement with simulated ones, which proves the feasibility of the concept. The design was developed with the help of ANSYS HFSS EM simulator.

II. FSS Unit Cell Design and Analysis

A. FSS Unit Cell Design

The FSS unit cell is simulated using ANSYS HFSS software, in which Floquet ports and periodic boundaries are adopted to simulate the design as an infinite structure. The diagram of the unit cell is depicted in Fig. 1, in which a square loop band stop FSS is selected due to its simplicity and symmetric structure for dual polarizations.

The square loop patch is printed on the top of the RT/Duroid 5880 substrate, thickness = 3.175mm, dielectric constant ε_r = 2.2, and loss tangent tan δ = 0.0009. Around the edge of each unit cell, a square loop channel is created to allow a grid being inserted and removed to control the capacitance between two adjacent units.

All the dimension parameters of the unit cell are listed in Table I. A clear transmission null is noticed at 4.6 GHz for this set of dimension parameters, as shown in Fig. 2. A slight shift was observed in the transverse electric (TE) and transverse magnetic (TM) responses respectively at 45°

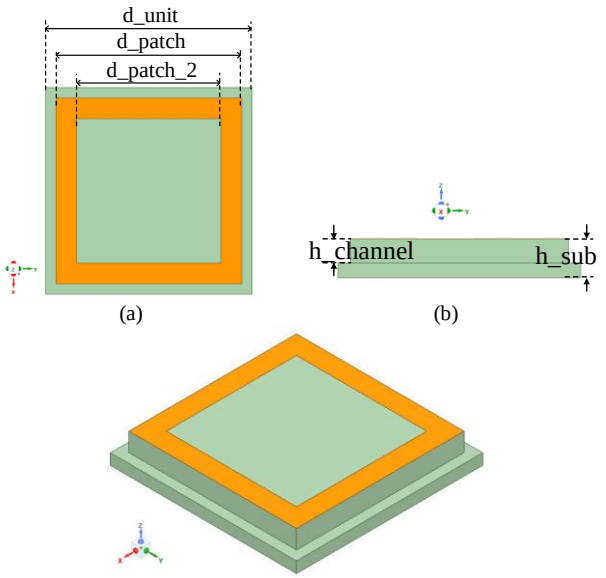

Fig. 1. (a) the top view and dimensions of the FSS cell. (b) the cross-sectional view. (c) the perspective view.

TABLE I. UNIT CELL DIMENSIONS

Parameter	d_unit	d_patch	d_patch_2
Value (mm)	20	18	14
Parameter	h_channel	h_sub	
Value (mm)	2	3.18	

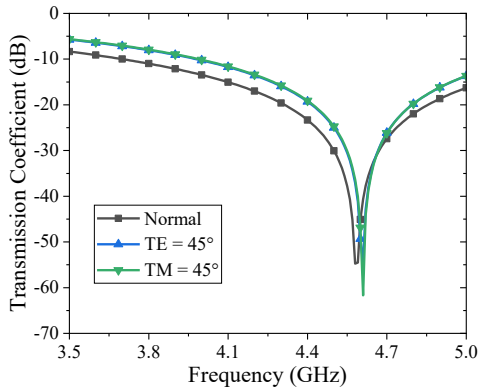

Fig. 2. Simulated transmission coefficient of the FSS.

angle from the normal response, although the difference is so small that could be neglected, which shows a good consistence of the basic FSS unit design regarding to the incident wave angle.

B. FSS Unit Cell with Grids Design and Analysis

After appropriately designing the FSS unit cell, two different types of grids of which the dimension matches that of the channels are simulated, as shown in Fig. 3. The first type is a pure dielectric grid as shown in Fig. 3(a), and the second type is a metal-dielectric grid developed from the first type by adding a metal layer at the bottom of the grid, as shown in Fig. 3(b).

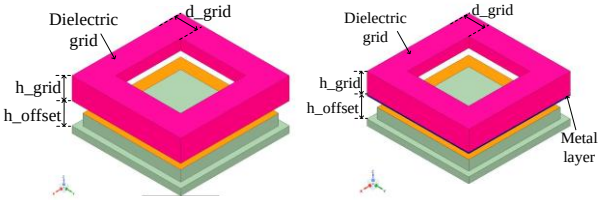

Fig. 3. Exploded view of the FSS unit with the (a) dielectric grid and (b) metal-dielectric grid.

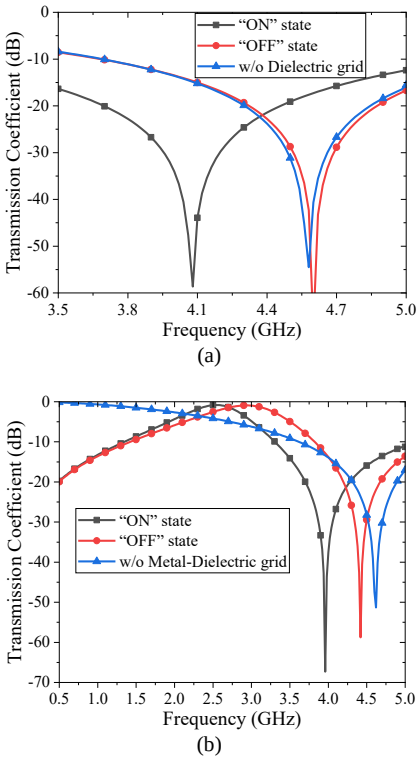

Fig. 4. Simulated transmission coefficient results for the FSS with (a) dielectric grid and (b) metal-dielectric grid.

Each of the two types is working at two states, namely "ON" and "OFF" states. The "ON" and "OFF" states are defined as h_offset = 0 mm, namely the grid connected with the FSS, and h_offset = 2 mm, namely the grid removed from the FSS, respectively. The width of the top grid (d_grid) is set to 4 mm. The height of the grid (h_grid) is set to 4 mm including 2 mm height matching with channels and additional 2 mm at top for extra capacitance. Notice that the width of bottom grid where should be matched with that of channels is reduced from 2 mm to 1.7 mm for processing tolerance in case the grid is not able to be fit in the channels.

The dielectric of the grid used in the simulation is set to be consistent with the standard 3D printing material called polylactic acid (PLA), which features the permittivity of 2.4 and low loss tangent [13]. As mentioned in Part A, the 3D-printed dielectric grid would compensate the reduction of the coupling capacitance introduced by the channels, thus increasing the effective permittivity of the whole

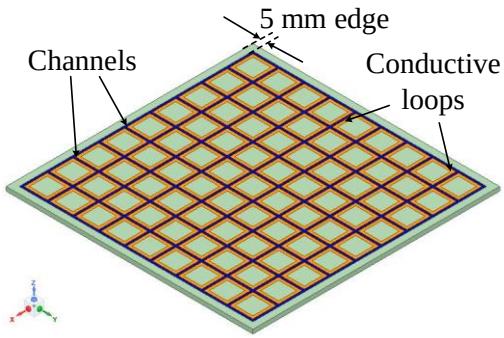

Fig. 5. The perspective view of the 9 × 9 FSS prototype with channels.

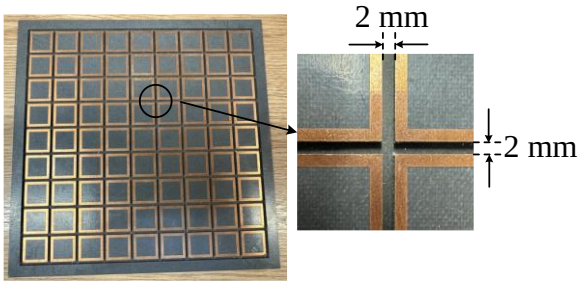

Fig. 6. The fabricated FSS with channels.

structure and decreasing the resonant frequency of the FSS. One could deduce that the higher the permittivity of the grid is, the higher the effective permittivity of the whole structure will be, meaning that the resonant frequency of the FSS could be further shifted to the lower frequency if the designers select higher permittivity materials. This could be another possible way to get larger frequency reconfigurability in the future designs.

The simulated transmission coefficient results of whole structure are shown in Fig. 4. As can be seen, the frequency response of dielectric grid is shifted from 4.6 GHz to 4.1 GHz for "ON" state, and nearly remains at 4.6 GHz for "OFF" state. The frequency response of metal-dielectric grid for "ON" state is shifted from 4.6 GHz to 4.0 GHz, and transmission at the lower frequency band is also suppressed due to the additional inductance introduced by the bottom metal layer. Similarly, the frequency response remains near 4.6 GHz for "OFF" state. Both simulation results are consistent with the theoretical analysis above, proving the reconfigurability and feasibility of the designs. In addition, based on the analysis in Part A, it could be expected that the frequency response for 45° angle incident wave would also be similar to the normal one, thus is not shown in the figures for the purpose of simplicity.

III. Fabrication and Measurement

A. Fabrication

The simulated 20 mm × 20 mm unit cell with channels is extended to a 9 × 9 array to create a prototype of the FSS, as shown in Fig. 5. A 5 mm width edge was added for robustness of the structure. A photograph of fabricated FSS with detailed channels is also shown in Fig. 6, in which the

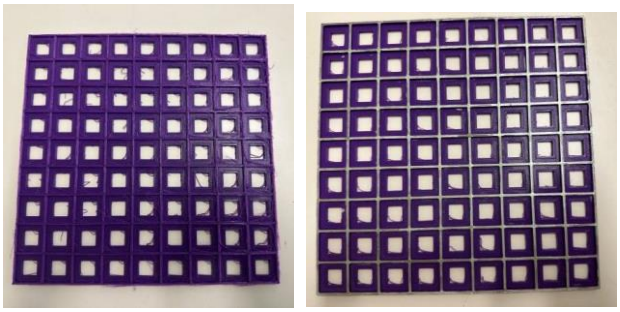

(a) (b)

Fig. 7. The 3D-printed grids. (a) Dielectric grid and (b) metal-dielectric grid.

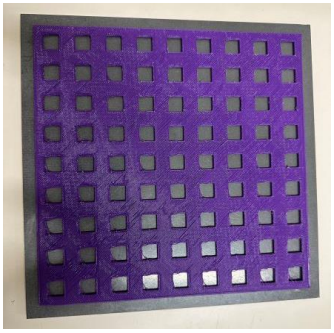

Fig. 8. The FSS mounted with the grid.

substrate around the square loop is partially removed to introduce the 2 mm height and width channels.

An Original Prusa i3 MK2.5S 3D printer [14] and a Raise3D E2 3D printer [15] were used to print the small part and full structure of the grid, respectively. The material used to print the grid is the standard polylactic acid (PLA), which has been widely applied in 3D printing industry due to its advantages of low cost, high robustness, and high reliability. The dielectric grid is directly printed from 3D printing, and the metal-dielectric grid is processed by painting a silver conductive layer onto one side of it [16]. The photograph of the two grids and that of full structure with FSS are shown in Fig. 7 and 8, respectively. Then the full structure were set up into the plane wave chamber to conduct the transmission coefficient measurement.

B. Measurement and Results

The measurement was conducted using the standard transmission measurement platform, as shown in Fig. 9. As can be seen, the measurement platform consists of a pair of transmitter/receiver antennas and surrounding absorbers, and the FSS under test is placed at the middle of the antenna pair, perpendicular to the plane wave direction.

The measurement results for two types of grids are shown in Fig. 10. As can be seen from Fig. 10(a), a clear frequency response at about 4.1 GHz is observed for dielectric grid for "ON" states, and results for both states match well with the simulation ones. As can be seen from Fig. 10(b), both frequency response at 4 GHz band and additional frequency response at lower frequency band are observed for metal-dielectric grid. The measurement

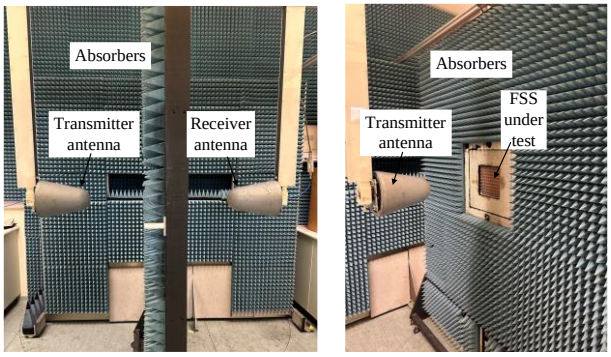

(a) (b)

Fig. 9. The photograph of the measurement platform.

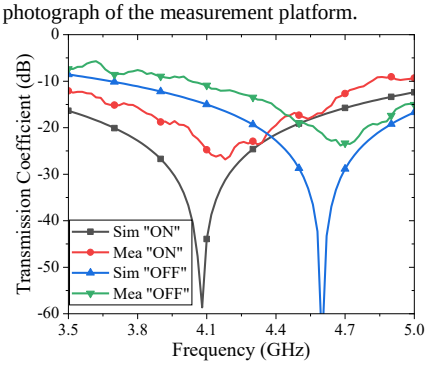

(a)

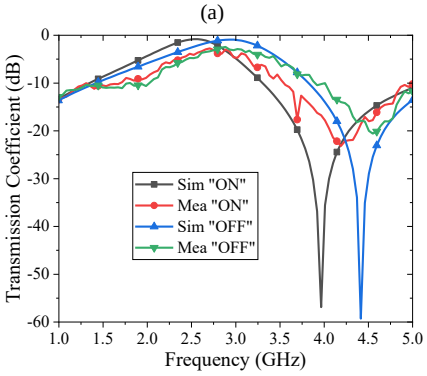

(b)

Fig. 10. Measured transmission coefficient results for the FSS with (a) dielectric grid and (b) metal-dielectric grid.

results for both dielectric and metal-dielectric grids show a reasonably good agreement between the simulation and fabrication, which prove the feasibility of the designs.

IV. Conclusion

This paper has presented a reconfigurable FSS structure using movable 3D-printed dielectric and metal-dielectric grids. Frequency reconfiguration has been achieved when the two types of 3D-printed grids are loaded into the FSS structure. A full structure combining the 9 × 9 FSS array with 3D-printed grids were fabricated and measured using standard transmission measurement platform to verify the performance. The measurement results show good agreement with simulations, which proves the frequency reconfigurability of the structure and the feasibility of the idea. Although the grid is moved manually in this design, our goal for the future designs is to apply piezo electric actuators such as those in [10] to achieve electrical controlling for the position of the grid. This could be a solution for frequency reconfigurable FSS and other periodic structure with the advantages of low-cost, ease-of-fabrication and high-flexibility, providing potential path for integration with other antenna designs.

Acknowledgment

The authors would like to thank Mr. Keith Greenhow and Joseph Hill for their help with 3D printing the grids. This work was funded by the EPSRC grant titled Low-Profile Ultra-Wideband Wide Scanning Multi-Function Beam-Steerable Array Antennas (EP/S005625/1), and Royal Society - International Exchanges 2019 Cost Share (NSFC) (Ref: IEC\NSFC\191780).

References

[1] R. Anwar, L. Mao, and H. Ning, "Frequency Selective Surfaces: A Review," Applied Sciences, vol. 8, no. 9, p. 1689, 2018-09-18 2018, doi: 10.3390/app8091689.

[2] B. A. Munk, Frequency selective surfaces: theory and design. John Wiley & Sons, 2005.

[3] I. S. Syed, Y. Ranga, L. Matekovits, K. P. Esselle, and S. G. Hay, "A Single-Layer Frequency-Selective Surface for Ultrawideband Electromagnetic Shielding," IEEE Transactions on Electromagnetic Compatibility, vol. 56, no. 6, pp. 1404-1411, 2014-12-01 2014, doi: 10.1109/temc.2014.2316288.

[4] Q. Chen, D. Sang, M. Guo, and Y. Fu, "Frequency-Selective Rasorber With Interabsorption Band Transparent Window and Interdigital Resonator," IEEE Transactions on Antennas and Propagation, vol. 66, no. 8, pp. 4105-4114, 2018-08-01 2018, doi: 10.1109/tap.2018.2835671.

[5] T. Deng, Y. Yu, Z. Shen, and Z. N. Chen, "Design of 3-D Multilayer Ferrite-Loaded Frequency-Selective Rasorbers With Wide Absorption Bands," IEEE Transactions on Microwave Theory and Techniques, vol. 67, no. 1, pp. 108-117, 2019-01-01 2019, doi: 10.1109/tmtt.2018.2883060.

[6] T.-W. Li et al., "A Novel Miniaturized Multiband Strong Coupled-FSS Structure Insensitive to Almost All Angles and All Polarizations," IEEE Transactions on Antennas and Propagation, vol. 69, no. 12, pp. 8470-8478, 2021-12-01 2021, doi: 10.1109/tap.2021.3063351.

[7] S. Pendharker, R. K. Shevgaonkar, and A. N. Chandorkar, "Optically controlled frequency-reconfigurable microstrip antenna with low photoconductivity," IEEE antennas and wireless propagation letters, vol. 13, pp. 99-102, 2014.

[8] N. Behdad and K. Sarabandi, "Dual-band reconfigurable antenna with a very wide tunability range," IEEE Transactions on Antennas and Propagation, vol. 54, no. 2, pp. 409-416, 2006.

[9] H. Sun and S. Sun, "A Novel Reconfigurable Feeding Network for Quad-Polarization-Agile Antenna Design," IEEE Transactions on Antennas and Propagation, vol. 64, no. 1, pp. 311-316, 2016-01-01 2016, doi: 10.1109/tap.2015.2497350.

[10] M. S. Rabbani, J. Churm, and A. P. Feresidis, "Continuous Beam-Steering Low-Loss Millimeter-Wave Antenna Based on a Piezo-Electrically Actuated Metasurface," IEEE Transactions on Antennas and Propagation, vol. 70, no. 4, pp. 2439-2449, 2022-04-01 2022, doi: 10.1109/tap.2021.3137248.

[11] J. Zhu, Y. Yang, N. Hu, S. Liao, and J. Nulman, "Additively Manufactured Multi-Material Ultrathin Metasurfaces for Broadband Circular Polarization Decoupled Beams and Orbital Angular Momentum Generation," ACS Applied Materials & Interfaces, vol. 13, no. 49, pp. 59460-59470, 2021/12/15 2021, doi: 10.1021/acsami.1c16493.

[12] J. Zhu et al., "Additively Manufactured Millimeter-Wave Dual-Band Single-Polarization Shared Aperture Fresnel Zone Plate

Metalens Antenna," IEEE Transactions on Antennas and Propagation, vol. 69, no. 10, pp. 6261-6272, 2021-10-01 2021, doi: 10.1109/tap.2021.3070224.

[13] C. Dichtl, P. Sippel, and S. Krohns, "Dielectric Properties of 3D Printed Polylactic Acid," Advances in Materials Science and Engineering, vol. 2017, pp. 1-10, 2017-01-01 2017, doi: 10.1155/2017/6913835.

[14] "Original Prusa i3 MK2.5S", prusa3d.com, 2022. [Online]. Available: https://help.prusa3d.com/tag/mk2-5s. [Accessed: 10- Oct- 2022]

[15] "IDEX 3D Printer | Precise, Reliable, Affordable - Raise3D E2", raise3d.com, 2022. [Online]. Available: https://www.raise3d.com/products/e2/. [Accessed: 10- Oct- 2022]

[16] "RS PRO Conductive Lacquer - RS components", uk.rs-online.com, 2022. [Online]. Available: https://uk.rs-online.com/web/p/electronics-varnishes/1863600. [Accessed: 10- Oct- 2022]